Laser and Particle Beams (1992), *vol.* 10, *no.* 1, *pp.* 65–74
Printed in the United States of America

X-ray emission from thin-foil laser-produced plasmas

By L. GIZZI,* D. BATANI,† V. BIANCALANA, A. GIULIETTI, AND D. GIULIETTI‡
Istituto di Fisica Atomica e Molecolare, CNR, Via del Giardino, 7, 56100 Pisa, Italy

(Received 18 September 1990)

We studied X-ray emission from laser plasmas produced by irradiation of thin plastic foils with 1.064-μm Nd laser light at intensity up to 2×10^{13} W/cm^2 with 3-ns pulses. The level of X-ray emission at different spectral windows was measured versus laser intensity and foil thickness. The electron temperature of the X-ray source was also measured. At intensity above 6×10^{12} W/cm^2 our data showed the formation of nonthermal tails in the X-ray spectrum, which has been related to two plasmon decay instability.

1. Introduction

The use of thin-foil targets is a well-known technique in laser plasma experiments for the production of long-scale-length, high-temperature plasmas. From an experimental point of view the advantage of using thin foils instead of thick solid targets is that in the latter case there are at all times complicated temperature and density profiles; in particular, there is always a layer of plasma at the critical density. With thin foils, on the contrary, the temperature in the plasma is approximately uniform, and after a given time t_{cr} the plasma becomes underdense. In addition, the evolution of the plasma parameters n_e and T_e can be evaluated with simple analytical self-similar models (e.g., London & Rosen 1986). These two features permit a better interpretation of experimental results.

Plasmas produced from thin foils have been used as a lasing medium in X-ray laser experiments (Matthews & Rosen 1988; Rosen *et al.* 1985). From the point of view of incoherent laser plasma X-ray sources the use of thin foils is interesting as well for both fundamental physics and applications. It is also a way to minimize target debris, which can be detrimental in various applications; this configuration is complementary to others already in use (Turcu *et al.* 1990). A limited number of investigations are presently available on X-ray emission studies from laser-irradiated thin targets, including those by Juraszek *et al.* (1990), Celliers & Eidmann (1990), and Eidmann *et al.* (1984).

In our experiment we irradiated thin plastic (Formvar) foils with a Nd laser and recorded X-ray signals with a filtered Si P-I-N detector. Owing to the low atomic numbers and to the spectral window of our filtered detector, we were able to measure a pure bremsstrahlung signal, with no contribution from line emission. This permitted us to measure the electron temperature T_e by the well-known method of recording the X-ray signal with the same detector but with different filters to reconstruct the slope of the bremsstrahlung spectrum (Jahoda *et al.* 1960).

Our data also showed the formation of a nonthermalized electron population at intensities $\geq 6 \times 10^{12}$ W/cm^2. Nonthermal tails in the X-ray spectra have already been observed from thin targets (Eidmann *et al.* 1984) and systematically studied with thick targets (see,

*Present address: Blackett Laboratory, Imperial College, London, UK.
†Present address: ICF Group, Dipartimento di Fisica, Universitá Statale di Milano, Italy.
‡Also at Dipartimento di Fisica, Universitá di Pisa, Italy.

 0263-0346/92 $5.00 + .00

for example, Amiranoff 1984). Several mechanisms of electron acceleration to suprathermal energies have been proposed to explain those observations. In our experiment the production of suprathermal electrons seems to be connected with two plasmon decay (TPD) instability, which was separately studied with optical time-resolved diagnostics (A. Giulietti *et al.* 1990; D. Giulietti *et al.* 1991).

2. Plasma production and diagnostics

The experimental apparatus is shown in figure 1 with two perpendicular views of the interaction chamber. A Nd laser ($\lambda = 1.064\ \mu$m, $E_L \leq 3$ J, $t_L = 3$ ns FWHM of a quasi-triangular pulse) was focused normally on a thin plastic foil target by an $f/8$ lens into a vacuum chamber. The focal spot diameter was $\approx 60\ \mu$m. Prepulse energy was kept below 10^{-4} the main pulse energy, and it was experimentally checked that this level could not produce any early plasma formation. X-ray emission was detected with a Si P-I-N diode (025-PIN-125 produced by Quantrad Corporation) filtered with Al filters of thickness between 1.6 and 13 μm. This detector was placed in the horizontal plane 20 cm from the plasma at 45° from the laser beam axis.

We also obtained images of our X-ray source with the help of a pinhole camera. It was positioned in different ways during the experiment, but always at an angle of 45° to the horizontal plane.

In the same experiment visible light emitted at 90° to the laser beam was spectrally and temporally resolved with a spectrometer coupled to a streak camera. Harmonic emission of 2ω and $3\omega/2$ was analyzed and used as a diagnostic of the underdense plasma. The 2ω spectrum was shifted owing to stimulated Brillouin scattering (SBS), and from the shift it

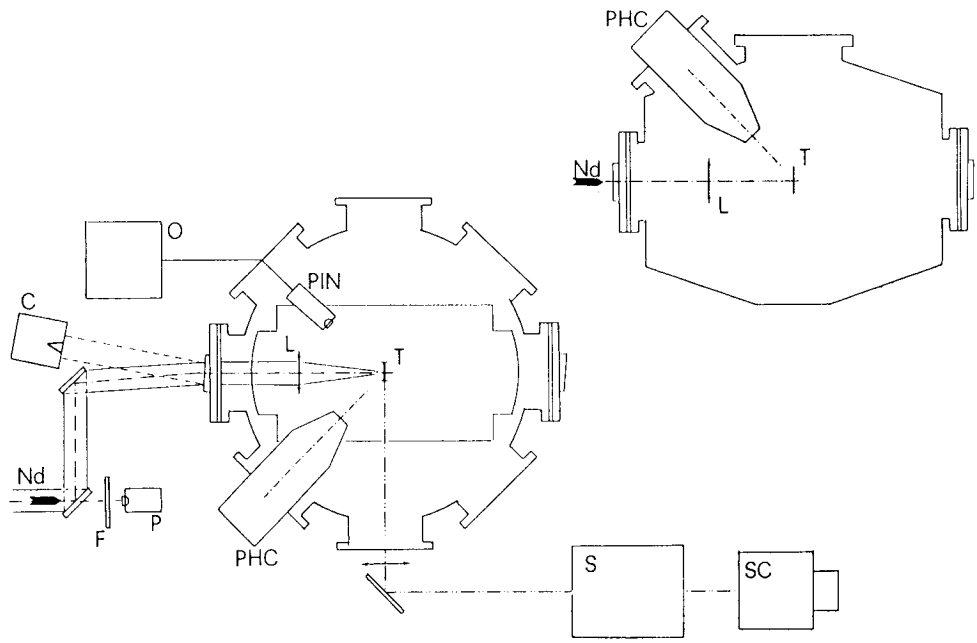

FIGURE 1. Layout of the experimental arrangement: PHC—pinhole camera; PIN—X-ray diode; T—target; L—focusing lens; C—calorimeter; P—photodiode; F—filter; O—oscilloscope; S—spectrometer; SC—streak camera.

was possible to determine the plasma temperature. Typical temperatures were 500 eV for foils of thickness ≈ 1 μm irradiated at intensity $I_L \approx 10^{13}$ W/cm^2 (A. Giulietti *et al.* 1989, 1990). Both TPD and SBS are nonlinear phenomena characterized by a threshold intensity. In our conditions we can reach this intensity only close to the peak of the laser pulse and hence when the plasma is hottest. At this time the plasma is well below critical, as deduced from self-similar models and determined experimentally.

3. X-ray emission data

Figure 2 shows X-ray diode signals recorded with a 6-μm Al filter versus laser intensity for foils of different thicknesses. Since the angular distribution of the X-ray source can be reasonably considered to be independent of both target thickness and laser intensity, we can consider those signals to be proportional to the emitted X-ray energy in the spectral range permitted by the filtered diode.

From figure 2 two regimes are apparent, depending on target thickness d: for $d \geq 0.5$ μm the X-ray signal is weakly dependent on foil thickness, while at $d \approx 0.2$ μm X-ray emission becomes much lower. Other evidence is that X-ray emission saturates at high I_L values.

Figure 3 shows X-ray signals obtained with a foil of 1.5-μm thickness with different Al filters in front of the detector. These data have been used to calculate the electron temperature of the X-ray source (see figures 5 and 7) and the laser to X-ray conversion efficiency (see figure 6).

Figure 4 (bottom) shows a typical pinhole image of the X-ray source from a 1.5-μm-thick foil target irradiated at 10^{13} W/cm^2. The camera was set as in the upper right part of figure 1. A 20-μm-diameter pinhole filtered with 1.6-μm-thick Al was used, and the pinhole camera magnification was 5. The image has roughly a circular shape with a 60-μm diameter; i.e., the size of the X-ray source is comparable with the laser spot size. This is consistent with X-ray emission occurring mainly from plasma densities well above critical, which is well established for plasma produced from thick solid targets (O'Neill 1988). An

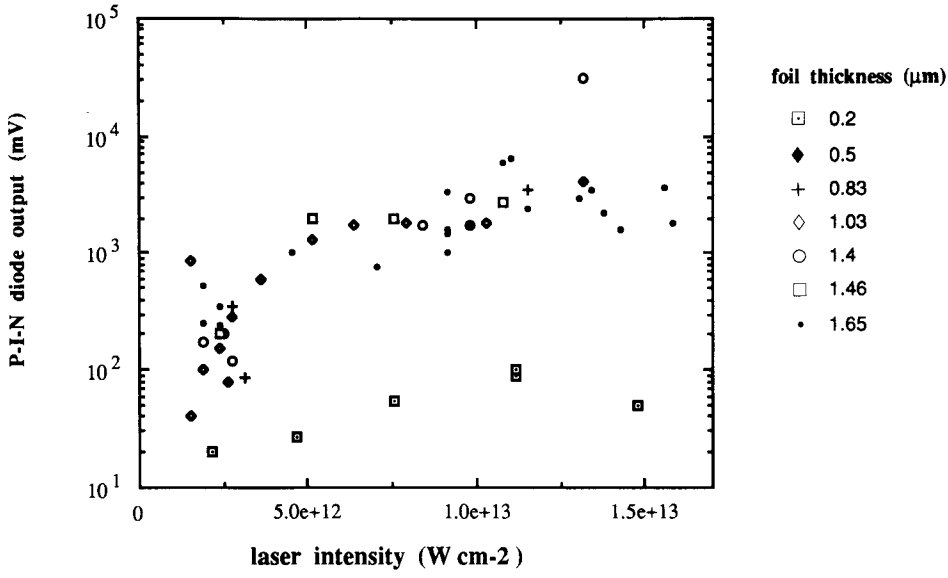

FIGURE 2. P-I-N diode signals versus intensity with a 6-μm Al filter for different target thicknesses.

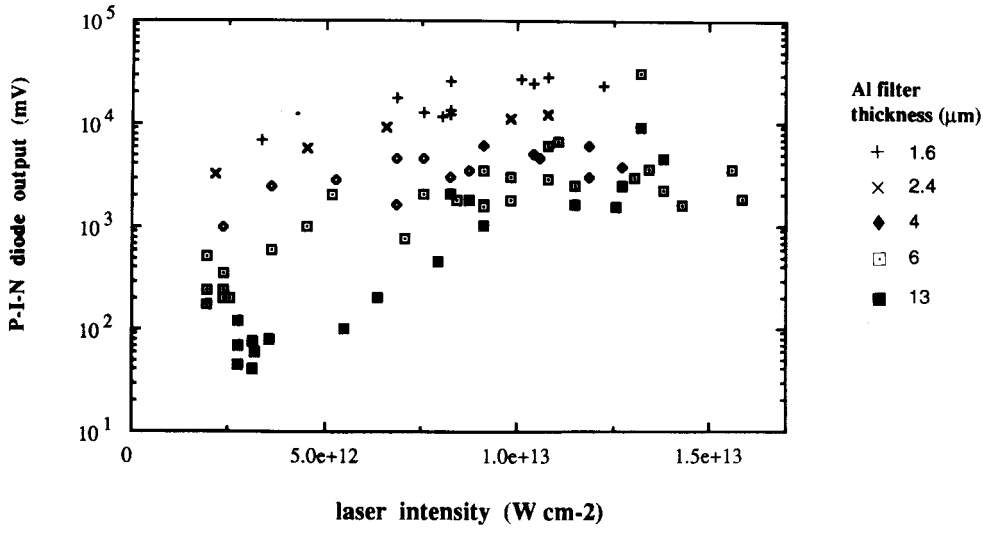

FIGURE 3. P-I-N diode signals versus laser intensity with a $d = 1.5$ μm foil target for Al filters of different thicknesses.

idealized shape of the plasma at the time when the maximum density is the critical one is shown, for 1.5-μm Formvar foil, in figure 4 (top), where the longitudinal size of the plasma is about twice the density scale length from the London & Rosen (1986) model.

For a small number of shots the prepulse to main pulse energy ratio was higher than 10^{-4}; in those cases it was not possible to measure any X-ray signal. This is consistent with the previous assumption that in the case of a large prepulse the early plasma formation caused the plasma to be underdense at the time of interaction with the main laser pulse. Similarly, with very thin foils ($d \approx 0.2$ μm), for which burnthrough is very early in the pulse, the X-ray emission was drastically reduced.

We could not directly measure the time duration of our X-ray pulse owing to the rise time of our P-I-N diode (2 ns) and the oscilloscope bandwidth (500 MHz).

4. Electron temperature and conversion efficiency

In our wavelength region the bremsstrahlung spectrum emitted from the plasma has the form

$$J(\lambda) = A_0\left(\frac{n_e^2}{\lambda^2\sqrt{T_e}}\right)\exp\left(-\frac{hc}{\lambda T_e}\right).$$

Hence from data in figure 3 one could calculate the electron temperature by taking into account that the P-I-N signal is proportional to

$$V_{\mathrm{pin}}(D, T_e) = B_0\int \lambda^{-2}\exp\left(-\frac{hc}{\lambda T_e}\right)\exp(-\mu\rho D)S(\lambda)d\lambda,$$

where D is the filter thickness and T_e, measured in energy units, is the temperature of thermalized electrons in the X-ray source; μ is the mass absorption coefficient of the filter and ρ is its density; and $S(\lambda)$ is the spectral sensitivity of the P-I-N diode. A_0 and B_0 are dimensional constants that take into account geometrical and physical factors. The inte-

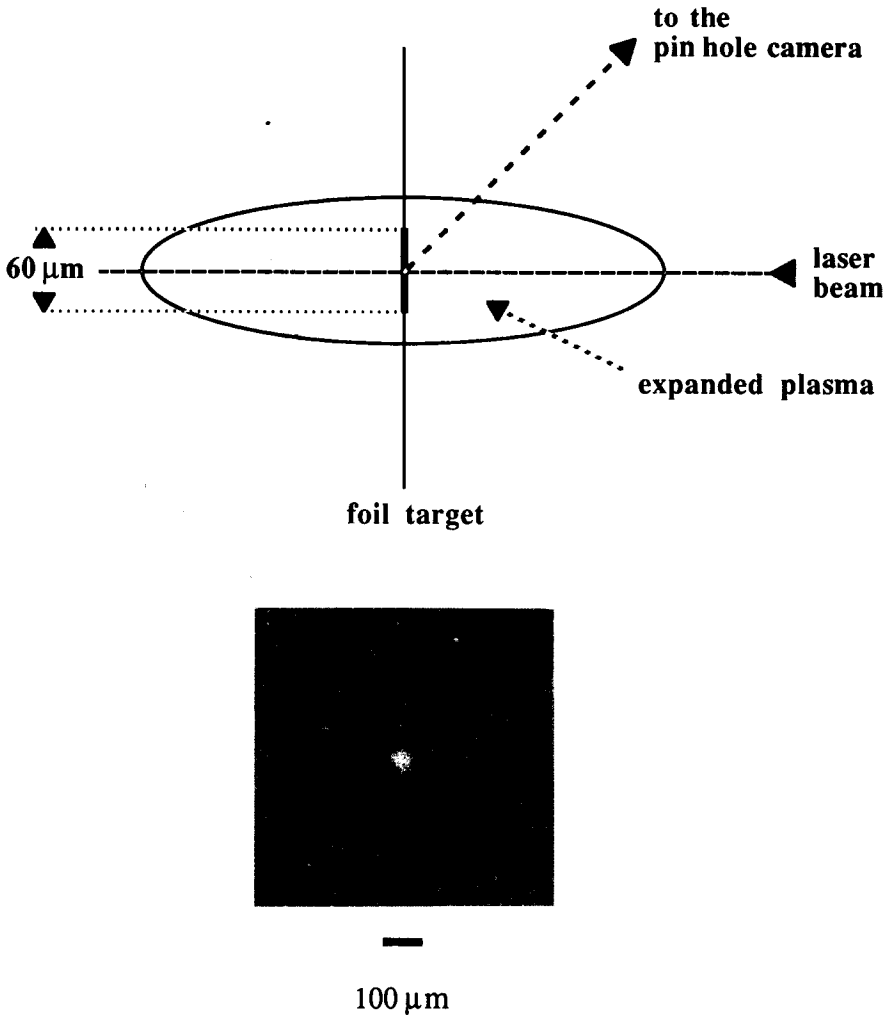

FIGURE 4. (bottom) Typical pinhole image on Kodak SB film recorded with a 20-μm-diameter pinhole filtered with 1.6-μm Al. The target foil thickness is $d = 1.5$ μm; and the laser intensity is 1.1×10^{13} W/cm^2. (top) Comparison of the laser spot size with the idealized plasma shape at the time at which the maximum density is the critical one.

gration limits were taken between 0.25 and 32 Å, and the integral was numerically evaluated. The measured values of V_{pin} reported in figures 2 and 3 agree fairly well with the values calculated from the previous formula, once the experimental conditions are taken into account to evaluate the constant B_0. We tried to determine T_e by interpolating the experimental values of figure 3 with curves of the form $y = ax^b$ and using the ratio between the signals obtained with each filter and those obtained with the 13-μm filter. Hence we obtained the plot of figure 5 for 1.5-μm-thick targets.

We see that the nominal "temperature" does not depend on the filter pair for $I_L \leq 6 \times 10^{12}$ W/cm^2 only. For higher intensities the temperature depends on filter pairs, and it is higher the closer to 1 is the ratio between the thickness of the "thin" and that of the "thick" filter. This result is easily interpretable in terms of creation of a subpopulation of hot electrons and hence in terms of a "hard" component in the X-ray spectrum (with $h\nu \gg T_e$) emerging from the ordinary bremsstrahlung spectrum. Actually, this component is prac-

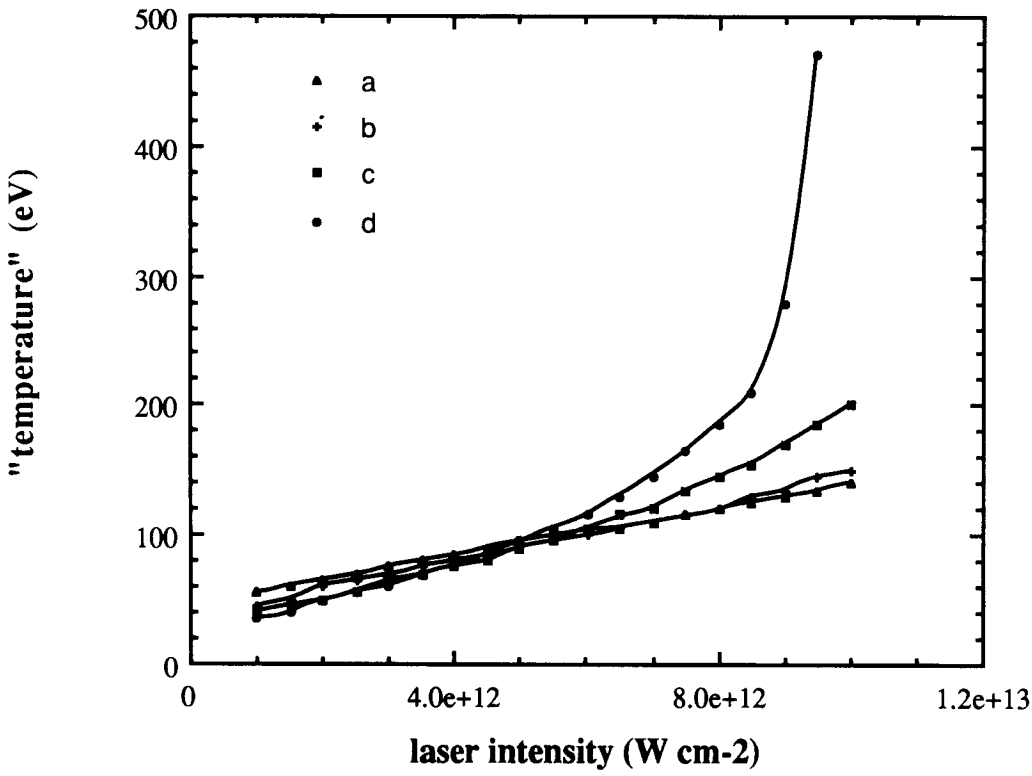

FIGURE 5. "Temperatures" versus intensity obtained with different Al filter pairs. The target foil thickness is 1.5 μm. Curve a refers to the (13 μm, 1.6 μm) filter pair, curve b to (13 μm, 2.4 μm), curve c to (13 μm, 4 μm), and curve d to (13 μm, 6 μm).

tically not attenuated by any of our filters. In this case, since the hard component is just a small part of the total X-ray spectrum, the plot from the 1.6- and 13-μm Al filter pair (curve a) is very close to the actual temperature. In Sec. 5 we will try to improve the accuracy of the cold-temperature evaluation versus intensity and to estimate the temperature of the hot-electron subpopulation.

We now consider the conversion efficiency $\eta = E_X/E_L$, i.e., the ratio between the soft-X-ray emitted energy in the wide spectral region permitted by Al filters and laser energy, respectively. Assuming an isotropic angular distribution, we find

$$E_X = \frac{4\pi Q_F(I_L)\tau_F}{S_0 \Delta\Omega},$$

where $Q_F(I_L)$ is the charge collected by the P-I-N diode at intensity I_L with a filter F, $S_0 \approx 6.2 \times 10^{-2}$ C/J is an average value of the P-I-N sensitivity in our spectral range, $\Delta\Omega$ is the solid angle subtended by the P-I-N diode, and τ_F is the filter-integrated transmissivity for the bremsstrahlung spectrum, defined as

$$\tau_F(D, T_e) = \frac{\int \exp\left(-\frac{hc}{\lambda T_e}\right) \exp(-\mu\rho D)\lambda^{-2}\, d\lambda}{\int \exp\left(-\frac{hc}{\lambda T_e}\right)\lambda^{-2}\, d\lambda}.$$

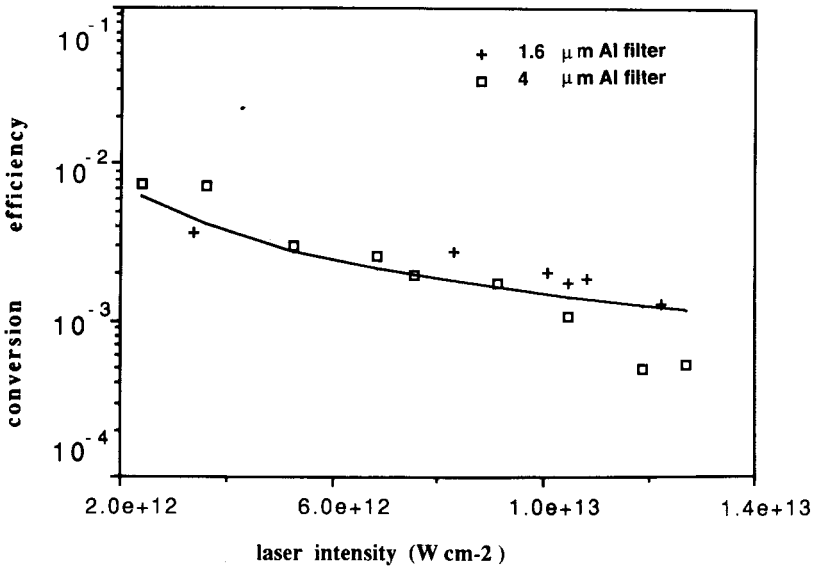

FIGURE 6. X-ray conversion efficiency versus laser intensity for 1.5-μm target foils.

In figure 6 we plot the efficiency η obtained from the experimental data for 1.6- and 4-μm Al filters. Efficiency is not very low if we consider that X-ray emission occurs during a period of time much shorter than the laser pulse, as deduced from data in Sec. 3. In view of application, higher efficiency can be obtained by an increase in both foil thickness and Z number of the target material.

From figure 6 we see that X-ray conversion efficiency $\eta = E_X/E_L$ decreases with laser intensity. This fact has already been observed by other authors, including Eidmann *et al.* (1984) and Celliers & Eidmann (1990). It is mainly a hydrodynamic effect that is easily understandable if we take into account that the thinner the foil or the higher the laser intensity, the sooner the plasma becomes undercritical. This effect was clearly shown by Juraszek *et al.* (1990), measuring the X-ray conversion efficiency of foils of different thicknesses at a fixed laser intensity. The solid curve in figure 6 fits the experimental data for a 4-μm-thick Al filter with a dependence $\eta \sim 1/I_L$ that can be deduced from the London & Rosen (1986) model. From the same model, assuming bremsstrahlung emission, we deduce values for the efficiency of the order of 10^{-3}, in rough agreement with those of figure 6.

5. Suprathermal tail in the electron population

5.1 *Data interpolation*

The temperature of about 500 eV measured from harmonic spectra (A. Giulietti *et al.* 1989; D. Giulietti *et al.* 1991) roughly corresponds to the "burnthrough temperature" T_{bt} of the London & Rosen model, i.e., the maximum temperature reached by the plasma during the laser pulse. On the other hand, the electron temperature T_e measured from X rays is lower and its dependence on laser intensity is stronger than that expected for T_{bt}, i.e., $T_{bt} \sim (I_L)^{1/3}$. This is clearly due to the fact that the X-ray emission occurs before the plasma becomes undercritical. Indeed, at early times, $T_e \leq T_{bt}$.

At nominal intensity $\geq 6 \times 10^{12}$ W/cm^2 our data suggest the presence of a suprathermal tail. Similar evidence is also reported in previous works (Eidmann *et al.* 1984; Amiranoff *et al.* 1982). We tried to evaluate the actual temperature T_e of "cold" electrons during the X-ray emission with a simple two-temperature model, resulting in the spectrum

$$J(\lambda) = A_0\left(\frac{n_e^2}{\lambda^2\sqrt{T_e}}\right)\exp\left(-\frac{hc}{\lambda T_e}\right) + A_0\left(\frac{n_e n_h}{\lambda^2\sqrt{T_h}}\right)\exp\left(-\frac{hc}{\lambda T_h}\right),$$

where n_h and T_h are, respectively, the density and the temperature of the hot component of an electron population with an assumed Maxwellian distribution. The P-I-N diode signal will be proportional to

$$V_{\text{pin}}(D, T_e) = B_0\int \lambda^{-2}\left[\exp\left(-\frac{hc}{\lambda T_e}\right) + R\exp\left(-\frac{hc}{\lambda T_e}\right)\right]\exp(-\mu\rho D)S(\lambda)d\lambda,$$

where $R = R(T_e, I_L)$ is the "weight" of the hard-X-ray tail. We used for T_h the function $T_h(I_L) \sim (I_L)^{1/2}$ (Amiranoff *et al.* 1982) and for $R(I_L)$ an exponential form that is well suited to reproduce a threshold behavior, i.e., practically no hot-electron generation for $I_L \leq 6 \times 10^{12}$ W/cm^2 and a rapid increase near the threshold (we are always very close to the threshold and far from saturation).

With these assumptions, and using a $T_e(I_L) \sim (I_L)^{2/3}$ law, as can be deduced from self-similar models, we obtained good data interpolation with the value $T_h \approx 15$ keV. The results of this interpolation are shown in figure 7. The value of T_h is largely dependent on our assumptions and hence must be considered only as an order of magnitude.

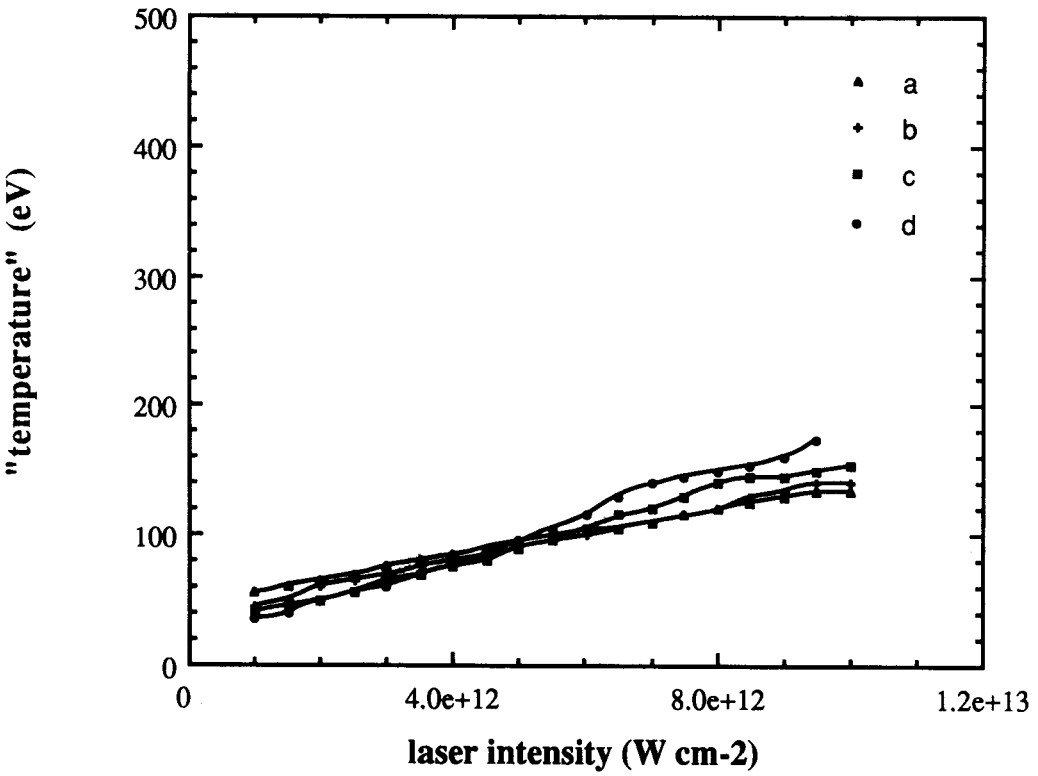

FIGURE 7. Thermalized electron temperature versus laser intensity obtained from the data of figure 5 after the interpolation taking into account the suprathermal population (see Sec. 5).

The agreement between plots from different filter pairs is definitely improved. Only for the "worst" filter pair (6 and 13 μm) is there still a discrepancy at the highest intensity. From figure 7 we can obtain a reasonable measurement of the temperature of the X-ray source at different laser intensities. Note that even at the highest laser intensities the temperature of the X-ray source is below 200 eV, much lower than the maximum plasma temperature measured during the interaction (500 eV).

A comparison of figure 7 with figure 5 (without the suprathermal correction) shows that the hypothesis of hot-electron generation at intensity above 6×10^{12} W/cm^2 is correct, even if a more accurate temperature plot needs a larger number of data and a quite sophisticated model taking into account a continuous temperature evolution during X-ray emission.

5.2 *Two plasmon decay and hot-electron generation*

We now briefly discuss the possible mechanism of electron extra-heating. The starting point is that the same intensity threshold was observed for both $3\omega/2$ emission (D. Giulietti *et al.* 1991) and the splitting of curves in figure 5. This finding suggests that hot electrons are produced by acceleration in Langmuir waves generated at $n_c/4$ in the TPD process. If this is true, the bulk of thermal soft X rays and the harder component of the spectrum are produced at different times and with different mechanisms.

It is well known that the interaction between a Langmuir wave (Chen 1984) propagating along x with a phase velocity v_ϕ and an electron with a velocity component v_x can efficiently accelerate the latter, provided that v_ϕ is comparable with v_x. This may produce electron energies that are orders of magnitude larger than the initial energy.

The maximum energy gain for an electron in the process is

$$\Delta E_{\max} = 2mv_\phi^2(v_E/v_\phi)^{1/2}[1 + (v_E/v_\phi)^{1/2}],$$

where v_E is the electron quiver velocity in the field of the Langmuir wave. Note that $v_E/v_\phi = (n^*/n_e)(\omega_p/\omega)^2 \approx n^*/n_e$, where n_e is the unperturbed electron density and n^* ($\leq n_e$) is the electron density variation associated with the Langmuir wave, which in turn determines its electric field through the Poisson equation. Hence the ratio between quiver and phase velocities nearly equates the relative wave amplitude. As a result of this process the electron velocity distribution will suffer the formation of a plateau around v_ϕ, whose width is about $\delta v = (8v_E v_\phi)^{1/2}$. Recalling that $v_\phi = v_T[3 + (k\lambda_D)^{-2}]^{1/2} > 3v_T$, we can easily understand that only Langmuir waves of relatively low phase velocity can appreciably affect the electron velocity distribution.

Assuming an initially Maxwellian electron velocity distribution of most probable velocity $v_T = (2KT_e/m)^{1/2}$ peak value, the key parameters of the phenomenon are the plasma temperature, the minimum value of v_ϕ in the Langmuir wave spectrum, and the wave amplitude. From those parameters we can evaluate the fraction of the electron population involved in the process and the maximum value $\Delta E_{\max}$ of the energy gain for this fraction.

In our experimental conditions the minimum value of v_ϕ is determined by Landau damping and is $v_{\phi_{\min}} \approx 3.6v_T$. With the reasonable assumption that $v_E/v_\phi \approx 10^{-1}$ we find $\delta v \approx 3v_T$. As a consequence, we can estimate a fraction of percent of suprathermal electrons with $\Delta E_{\max} \approx 15$ keV. These values are consistent with the values used in the numerical computation.

6. Conclusion

We have studied X-ray emission from plasmas produced by laser irradiation of thin plastic foils. From the X-ray intensity measurements, we observed that most of the X rays are

emitted early in the laser pulse when the plasma is still overdense, as is also shown by the shape of the source obtained with the pinhole camera and by the difference between the electron temperature T_e measured with X-ray diagnostics and that measured with visible diagnostics.

A tail of suprathermal electrons is generated during the laser pulse at "nominal" intensities $I_L \geq 6 \times 10^{12}$ W/cm^2. This is very close to the observed threshold for $3\omega/2$ emission, which in turn is a clear signature of TPD. It is reasonable to attribute the acceleration of suprathermal electrons to plasmons created by TPD. If this is true, the suprathermal tail is produced much later than the main X-ray pulse.

It is very difficult to evaluate the actual laser intensity in the focal region, but it is likely to be considerably higher than its nominal value of $I_L \leq 2 \times 10^{13}$ W/cm^2, owing to filamentation of the laser beam in the plasma. An evaluation of TPD threshold in our experimental conditions (D. Giulietti *et al.* 1991) gives $I_L \approx 10^{14}$ W/cm^2, a value that may be reached inside the filaments when the nominal intensity is of the order of 10^{13} W/cm^2. The presence of filamentation in our experiment was indirectly evidenced through the experimentally observed 2ω side emission, predicted by the theory in the presence of filamentation (Stamper *et al.* 1985).

Acknowledgments

We thank Silvano Bartalini, Istituto di Fisica Atomica e Molecolare, who built the pinhole camera used in our experiment and was always very helpful. We are also grateful to Dr. O. Willi for a critical reading of the manuscript and to P. Chessa for a contribution to its editing. This work was fully supported by Consiglio Nazionale delle Ricerche (Italy).

REFERENCES

AMIRANOFF, F. 1984 Thèse, Université Paris-Sud, Orsay, France.

AMIRANOFF, F. *et al.* 1982 *J. Phys.* (Paris) **43**, 1037.

CELLIERS, P. & EIDMANN, K. 1990 *Phys. Rev. A* **41**, 3270.

CHEN, F. 1984 *Introduction to Plasma Physics* (Plenum, New York), Chap. VII.

EIDMANN, K. *et al.* 1984 *Phys. Rev. A* **30**, 2568.

GIULIETTI, A. *et al.* 1989 *Phys. Rev. Lett.* **63**, 5244.

GIULIETTI, A. *et al.* 1990 In *Laser Interactions and Related Plasma Phenomena, Vol. 9*, pp. 273–285, H. Hora & G. H. Miley, eds. (Plenum, New York).

GIULIETTI, D. *et al.* 1990 Il Nuovo Cimento, 1991 (in press).

JAHODA, F. C. *et al.* 1960 *Phys. Rev.* **119**, 3.

JURASZEK, D. *et al.* 1990 Book of Abstracts, 20th European Conference on Laser Interaction with Matter, Schliersee, January 22–26, 1990, p. 66. Garching, Germany: Max-Planck Institut für Quantenoptik.

LONDON, R. A. & ROSEN, M. D. 1986 *Phys. Fluids* **29**, 3813.

MATTHEWS, D. L. & ROSEN, M. D. 1988 *Sci. Am.* **259 (6)**, 60.

O'NEILL, F. 1988 In *Laser Plasma Interactions 4, Proceedings of the 35th Scottish Universities' Summer School in Physics*, M. B. Hooper, ed., SUSSP Publications, Edinburgh, Scotland.

ROSEN, M. D. *et al.* 1985 *Phys. Rev. Lett.* **54**, 2.

STAMPER, J. A. *et al.* 1985 *Phys. Fluids* **28**, 8.

TURCU, I. E. *et al.* 1990 *Proc. Soc. Photo-Opt. Instrum. Eng.* **1278**, 32.